



Partial surface phase transformation of Li_3VO_4 that enables superior rate performance and fast lithium-ion storage

Xiaoqing Liu¹ · Liping Li¹ · Guangshe Li¹

Received: 13 August 2019 / Revised: 19 September 2019 / Accepted: 23 September 2019 / Published online: 6 December 2019
© The Nonferrous Metals Society of China 2019

Abstract

Li_3VO_4 is a promising electrode material for next-generation lithium-ion batteries (LIBs) due to its excellent specific capacity (592 mAh g^{-1}), suitable discharge voltage (0.5–1.0 V), and moderate volume change upon charge/discharge, while it still suffers from low electronic conductivity that usually gives a poor rate capability, low initial coulombic efficiency, and large polarization, imposing a challenge on its practical applications. In this work, a partial surface phase transformation of Li_3VO_4 was initiated via a freeze-drying method followed by a heat treatment in inert gas. Using this method, Li_3VO_4 was integrated with a conductive layer LiVO_2 and carbon matrix. The synergistic effect among Li_3VO_4 , LiVO_2 layer, and carbon matrix was systematically studied by optimizing the treatment conditions. When treated at 600°C in Ar, Li_3VO_4 -based composite delivered outstanding electrochemical properties, as expressed by a specific capacity (689 mAh g^{-1} at 0.1 A g^{-1} after 100 cycles), rate performance (i.e., 448 mAh g^{-1} at 2 A g^{-1}), and longtime cycle stability (523 mAh g^{-1} after 200 cycles at 0.2 A g^{-1}), which are superior to those without LiVO_2 conductive layer when treated at the same temperature in air. The findings reported in this work may offer novel hints of preparing more advanced anodes and promote the applications of vanadate materials such as Li_3VO_4 for next-generation lithium-ion batteries.

Keywords Li_3VO_4 · LiVO_2 · Rate performance · Electronic conductivity · Li^+ diffusion

1 Introduction

With the rapid increase of energy demand and environmental pollution, it is very important to explore clean and sustainable storage devices equipped with a fascinating energy density and power density [1–5]. Among various energy storage technologies, lithium-ion batteries (LIBs), owing to its fascinating energy density, long cycling lifespan and small memory effect, have evoked extensive attention over past decades [6, 7]. Graphite is widely used as commercial anode materials with a negligible volume expansion during the lithiation/delithiation process. However, the growth of lithium dendrites at low potential platform ($\sim 0.2 \text{ V}$) and low specific capacity (372 mAh g^{-1}) make it unable to keep up with the increasing demand for new-generation LIBs [8–10].

Thus, it is inevitable to exploit advanced alternatives with the high specific capacity to substitute the graphite anode.

Currently, Li_3VO_4 is deemed as one of the most promising anode materials, attributed to the following reasons: (i) a more considerable capacity (394 mAh g^{-1}) compared with graphite and $\text{Li}_4\text{Ti}_5\text{O}_{12}$, which only deliver 372 mAh g^{-1} and 175 mAh g^{-1} , respectively. Furthermore, the capacity can achieve 592 mAh g^{-1} when three Li ions reversibly insert in the Li_3VO_4 lattice [11, 12]; (ii) a high voltage platform ($\approx 0.75 \text{ V}$ vs. Li/Li^+ in average) that can efficiently inhibit the formation of lithium dendrites [13]; (iii) a small volume expansion of only 4% during the cycling process [14]. Unfortunately, the unsatisfying electrochemical properties such as the poor rate performance and large polarization resulted from low intrinsic electronic conductivity severely restrict its practical applications [15–17]. A few serious efforts were taken to solve this drawback, for instance: (i) enhancing electrical conductivity by combining with conductive carbonaceous matrix such as organic carbon, graphite, graphene, etc.; Ni et al. [18] prepared $\text{Li}_3\text{VO}_4/\text{N}$ -doped carbon, which exhibited unprecedented cycling stability (264 mAh g^{-1} after 2000 cycles at 2 A g^{-1}), due to the

✉ Guangshe Li
guangshe@jlu.edu.cn

¹ State Key Laboratory of Inorganic Synthesis and Preparative Chemistry, College of Chemistry, Jilin University, Changchun 130012, China

improved lithiation degree and electronic conductivity; (ii) modulating the electronic structure through aliovalent ion doping and introducing oxygen defects: Fe-doped Li_3VO_4 , reported by Liu et al. [19], delivered an outstanding rate capability, long lifetime cycling, which was mainly attributed to the formation of oxygen vacancies, reduced band-gap and fast Li^+ diffusion; (iii) reducing the particle size or designing the specific morphology to shorten the diffusion path of Li^+ and improve reaction activity: Shen et al. [20] synthesized highly homogeneous carbon-coated Li_3VO_4 spheres by a morphology inheritance route, showing a high capacity, excellent cycle stability and superior rate capability (reversible capacity are 287 mAh g^{-1} at a current rate of 20 C). Among these improved methods, hybridization with carbon is regarded as an easy and low cost method to achieve maximum benefits. In the meantime, LiVO_2 , as an analog of Li_3VO_4 , which is deemed as the excellent ionic and electronic conductivity materials, becomes the suitable materials for hybridization with Li_3VO_4 [21–23].

Herein, we integrated Li_3VO_4 with LiVO_2 and carbon by calcination at different temperatures in an inert atmosphere. Such a unique design combines some prominent merits: (i) LiVO_2 , an excellent ionic and electronic conductivity material, plays a critical role in accelerating electron transfer and Li^+ diffusion upon charge/discharge; (ii) introduction of the carbonaceous matrix can not only boost electron transfer but also suppress aggregation of particles during cycling. Because of these advantages, LL@C-600 (annealed in an inert atmosphere of Ar at $600 \text{ }^\circ\text{C}$) delivers a high specific capacity of 689 mAh g^{-1} after 100 loops at a current density of 100 mA g^{-1} and outstanding rate performance of 448 mAh g^{-1} at the current density of 2 A g^{-1} , which is superior to the previously reported Li_3VO_4 @carbon composites. These results further manifest that surface modified Li_3VO_4 is one of the most promising electrode materials for new-generation high-power density LIBs.

2 Experimental

2.1 Sample syntheses

2.1.1 Li_3VO_4 with a conductive surface layer

$3 \text{ mmol LiOH}\cdot\text{H}_2\text{O}$ and $1 \text{ mmol VO}(\text{acac})_2$ were dissolved in 20 ml of distilled water under stirring. Later, the obtained clear solution was freeze-dried for 2 days, and a brownish yellow floc was formed. At last, the above products were grinded, and annealed in an inert atmosphere of Ar at given temperatures (e.g., $550 \text{ }^\circ\text{C}$, $600 \text{ }^\circ\text{C}$ and $650 \text{ }^\circ\text{C}$) for 2 h at a heating rate of 5° min^{-1} to form Li_3VO_4 with a conductive surface layer. The corresponding samples were named as LL@C-550, LL@C-600 and LL@C-650, respectively.

2.1.2 Reference sample of Li_3VO_4 without a conductive surface layer

Using the above preparation procedure except for the treatment atmosphere, pure Li_3VO_4 was obtained by annealing in air at $600 \text{ }^\circ\text{C}$ for 2 h. The obtained sample was named as LVO.

2.2 Sample characterization

The sample structure was investigated by X-ray diffraction (XRD) on a Rigaku MiniFlex II X-ray diffractometer. The morphologies information of samples were examined by field emission scanning electron microscope (SEM, JEOL, model JSM-6700F) and transmission electron microscopy (TEM) images on a Tecnai G2S-TwinF20 apparatus. Raman spectra of the samples were recorded by a Renishaw Micro-Raman system. The chemical valence analysis of samples was performed using by X-ray photoelectron spectroscopy (XPS) with Al K α radiation (1486.6 eV) as the X-ray source.

2.3 Electrochemical measurements of samples

The electrochemical performances of the samples were tested by CR2025-type coin cells. The electrodes were constructed in several steps below. The active materials were dried in a vacuum oven at $100 \text{ }^\circ\text{C}$ for 12 h. Then, active materials, carbon black, and binder at a weight ratio of 7:2:1 were mixed in *N*-methyl-2-pyrrolidinone (NMP) to form a slurry. The slurry obtained was coated onto a copper foil and dried in vacuum for about 12 h. The cells were assembled in a glove box (the volume fraction of H_2O and $\text{O}_2 < 1 \times 10^{-5}\%$). $1 \text{ mol L}^{-1} \text{ LiPF}_6$ in ethylene carbonate and dimethyl carbonate (1:1 volume ratio) was used as electrolyte and the lithium metal as the reference electrode. The assembled cells were measured by a Neware battery test system. Cyclic voltammetry was obtained by an electrochemical workstation (CHI660C) at a scan rate of 0.2 mV s^{-1} . The electrochemical impedance spectrum (EIS) was recorded in a frequency range of 100 kHz – 0.01 Hz .

3 Results and discussion

3.1 Formation of Li_3VO_4 with a conductive layer LiVO_2 via partial surface phase transformation

Partial surface phase transformation of Li_3VO_4 was highly possible when treated at a high temperature in the inert atmosphere, since under such conditions there may exist a valence reduction such as from V^{5+} to V^{3+} . To examine this possibility, the preparation conditions were systematically studied by optimizing the treatment temperature in an inert

atmosphere. Figure 1 shows the powder XRD patterns of the samples treated at different temperatures in an inert atmosphere of Ar. It is shown that most of the diffraction peaks are identical to those for the orthorhombic structure of Li_3VO_4 (JCPDS, No. 38-1247), while other three extra diffraction peaks located at two theta of 18° , 48° and 68° , respectively. The extra ones were well attributed to LiVO_2 (JCPDS, No. 73-2047), indicating that (i) Li_3VO_4 -based composite was formed by integrating with LiVO_2 , and (ii) vanadium species

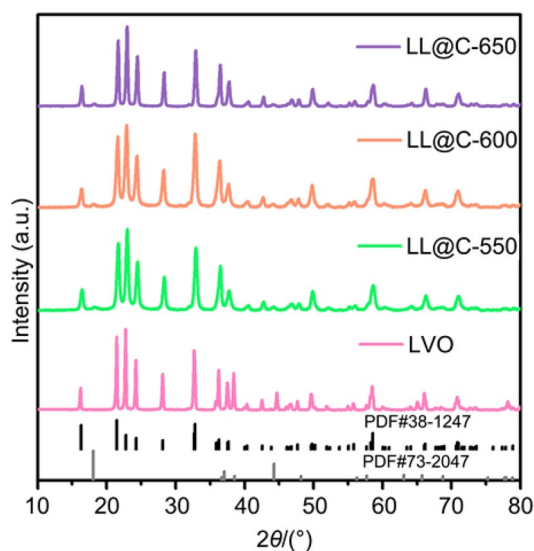


Fig. 1 Powder XRD patterns of the samples treated at different temperatures (marked as LL@C-550, LL@C-600, LL@C-650) in an inert atmosphere of Ar and at a fixed temperature of 600°C (marked as LVO) in air. The standard diffraction data for Li_3VO_4 (JCPDS, No. 38-1247) and LiVO_2 (JCPDS, No. 73-2047) were also given for comparison

were reduced to low valence state likely by organic carbon at high temperatures in the inert atmosphere, as reported elsewhere [24]. Varying the treatment temperature did not change peak positions of both components, but the relative intensities.

The phase composition for Li_3VO_4 when treated at a high temperature in inert atmosphere is further confirmed by examining the Raman spectra of LL@C-600, since Raman spectroscopy is sensitive to the lattice variations of materials. As shown in Fig. 2a, there are a D-band and a G-band located at 1348 cm^{-1} and 1586 cm^{-1} , respectively, which are both typical peaks of carbon. Interestingly, the peak intensity ratio of D band to G band (I_D/I_G) is about 0.81, manifesting a high graphitization degree of carbon, as reported by others [25, 26]. Such a graphitization appears necessary to promote the electronic conductivity of Li_3VO_4 . The existence of orthorhombic Li_3VO_4 was indicated by the magnified Raman spectrum in the wavenumber region of $200\text{--}1000\text{ cm}^{-1}$ (inset of Fig. 2a). In addition, the broadened and overlapped Raman signals in the region of $250\text{--}450\text{ cm}^{-1}$ cannot be well distinguished, indicating a mixed phase of Li_3VO_4 and LiVO_2 , according to Ref. [21].

All sample characterizations mentioned above demonstrate that when treated at a high temperature in the inert atmosphere, Li_3VO_4 could be achieved by integration with a conductive layer LiVO_2 and carbon matrix. It is well established that the appearance of the surface coating could affect the morphology, which can be very important for the electrochemical performance. SEM image of pristine Li_3VO_4 is shown in Fig. 3a. Particles of the sample LVO exhibit an irregular morphology and a non-uniform particle distribution, which also tend to agglomerate. Figure 3b–d display SEM images of the samples when varying the treatment

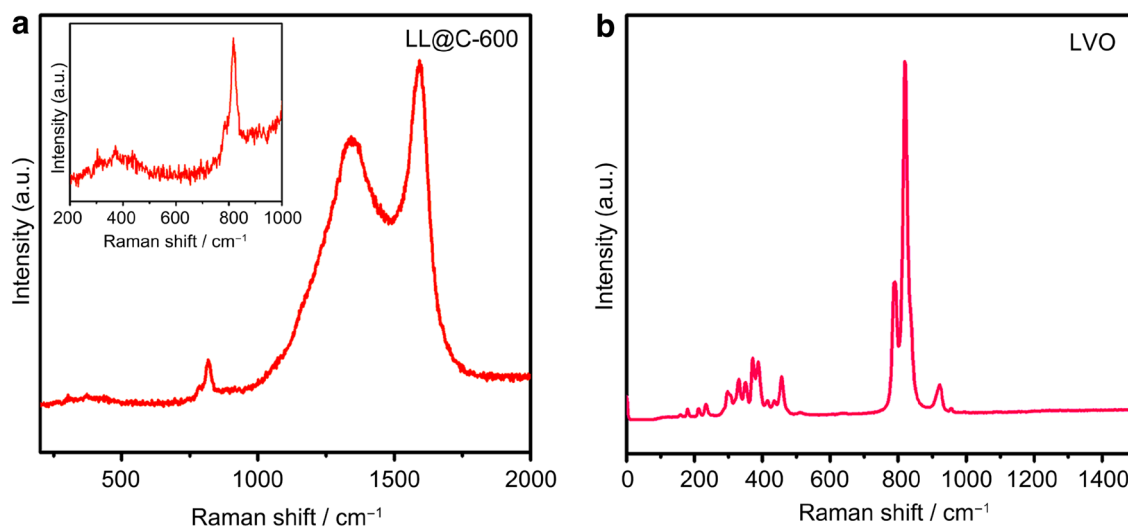


Fig. 2 Raman spectra of samples treated at 600°C **a** in inert atmosphere (LL@C-600) and **b** in air (LVO). Inset of **a** is an enlarged view of $200\text{--}1000\text{ cm}^{-1}$ of LL@C-600

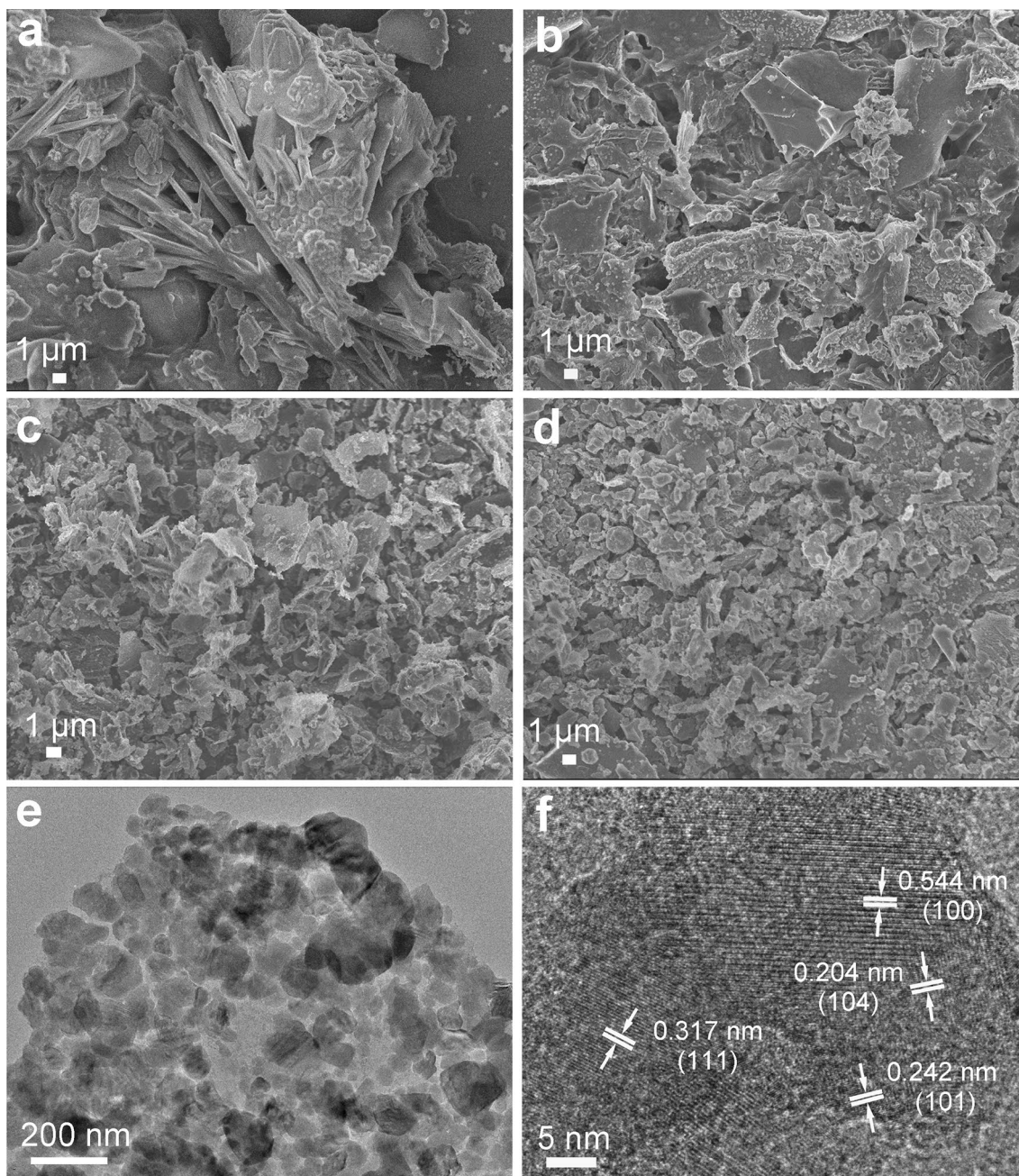


Fig. 3 SEM images of **a** the sample treated at a fixed temperature of 600 °C (marked as LVO) in air and **b–d** samples treated at different temperatures (marked as LL@C-550, LL@C-600, LL@C-650) in an inert atmosphere of Ar; **e** TEM image and **f** HRTEM image of LL@C-600

temperature in the inert atmosphere. All samples are composed of uniform sheet-like morphologies, especially when the treatment temperature is set at 600 °C (Fig. 3c). The uniform particles are believed to play a significance role in promoting the electrochemical properties of Li_3VO_4 , for instance in enhancing the cycling stability to a great extent, which would be described later. Careful data examination showed that the sheet-like morphology is inclined to agglomerate obviously to form chunks as the treatment

temperature increases. Figure 3e gives the TEM image of LL@C-600. The sheet-like morphology was composed of many small particles, and a mass of nanopores between particles were also revealed. The high-resolution TEM (HRTEM) image is displayed in Fig. 3f. The lattice spacings of 0.317 nm and 0.544 nm were assigned to the crystal planes (111) and (100) of Li_3VO_4 , respectively. Besides, the interplanar spacings of 0.242 nm and 0.204 nm were associated with the planes (101) and (104) of LiVO_2 ; manifesting

that V^{5+} was reduced to the low valence state of vanadium by carbon matrix during the heat-treatment process in inert atmosphere. A part of Li_3VO_4 was transformed into $LiVO_2$ phase, which is consistent with the XRD analysis.

To make sure that partial phase transformation occurred at surface, XPS was employed to study the surface chemical states and chemical components. Figure 4a shows the XPS data for Li_3VO_4 , in which the signals located at binding energies of 517.7 and 525.2 eV matched well with those for $V 2p_{3/2}$ and $V 2p_{1/2}$ of V^{5+} , as reported in literature [17, 27, 28]. The weak peak at 523.5 eV is in line with an X-ray satellite signal of O 1s [27–29]. Compared to the characteristic XPS signals for LVO, there appeared additional XPS signals at 516.3, 517.0, 523.6, and 524.3 eV when treated in inert atmosphere. The signals at 516.3 and 523.6 eV correspond to the spin–orbit splitting of $V 2p_{3/2}$ and $V 2p_{1/2}$ of V^{3+} , while the signals at 517.0 and 524.3 eV are in accordance with the assignments of V^{4+} as reported earlier [2, 29]. The appearance of the low valence state demonstrates that V^{5+} was reduced by carbon matrix during the heat-treatment process in inert atmosphere, in accordance with our XRD and HRTEM analyses.

3.2 Formation of Li_3VO_4 without a conductive layer

When treated in air at a high temperature, no conductive layer was formed, but the pure phase Li_3VO_4 . This is confirmed by XRD and Raman spectra. As shown by XRD data in Fig. 1, all diffraction peaks of LVO are identical to those of the orthorhombic structure of Li_3VO_4 (JCPDS 38-1247), while traces of impurity phases were absent. The formation of the pure phase of orthorhombic Li_3VO_4 is clearly demonstrated by the typical Raman signals appeared in the

wavenumber region of 250–900 cm^{-1} (Fig. 2b), as reported elsewhere [30]. In the following, the sample without a conductive layer would be used as the reference for comparative studies.

3.3 Optimum electrochemical performance of Li_3VO_4 via a conductive layer

Electrochemical performance of Li_3VO_4 with and without a conductive layer was comparatively studied. Figure 5a displays the initial discharge–charge curves for samples LVO and LL@C (550 °C, 600 °C, 650 °C) with the potential range of 0.01–3 V at a rate of 100 $mA g^{-1}$. As indicated by the similar discharge/charge curves, all samples exhibited the same electrochemical processes, while the initial capacities are totally different: the initial discharge/charge capacities of LVO samples are only 421/262 $mAh g^{-1}$. Comparatively, for LL@C-550, LL@C-600 and LL@C-650 electrodes, the first discharge/charge capacities are much higher, which are 938/561, 1036/678, and 651/405 $mAh g^{-1}$, respectively. The dramatically increased capacity is mainly ascribed to the synergistic effect of the conductive surface layer $LiVO_2$ and carbon matrix. The 1st, 2nd, 10th, 30th, 50th and 100th charge–discharge voltage curves of the LL@C-600 electrode over a potential range between 0.01 V and 3 V at a current density of 100 $mA g^{-1}$ are presented in Fig. 5b, in which the galvanostatic charge–discharge curves after the first cycle are overlapped well, implying a favorable reversibility of the electrode material upon charge/discharge [31, 32].

The existence of the conductive layer $LiVO_2$ in the LL@C-600 electrode does not change the electrochemical reaction processes, as demonstrated by the similar voltage curves after the first cycle for both LVO and LL@C-600

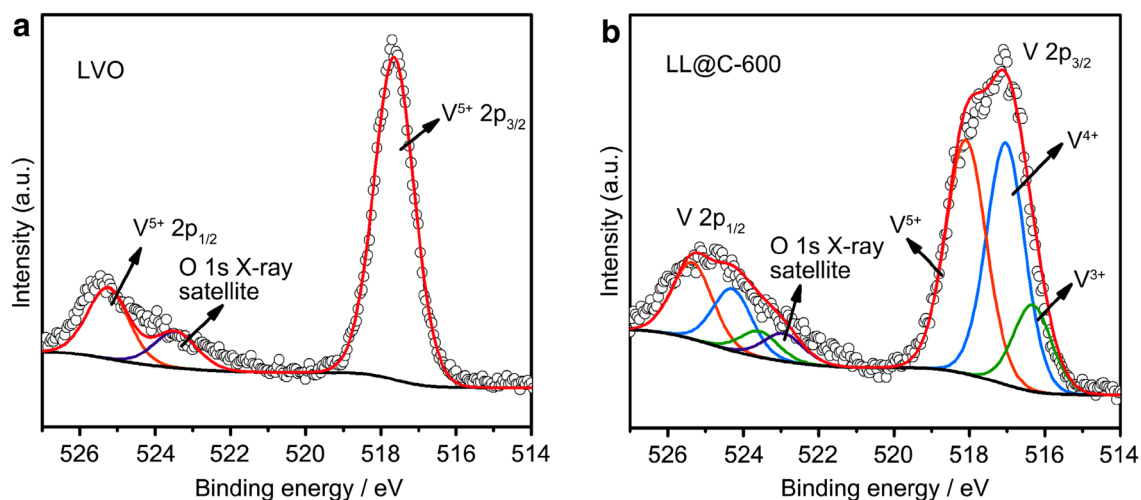


Fig. 4 High-resolution V 2p spectra and the corresponding fitting curves for samples treated at 600 °C **a** in air (marked as LVO) and **b** in the inert atmosphere (marked as LL@C-600)

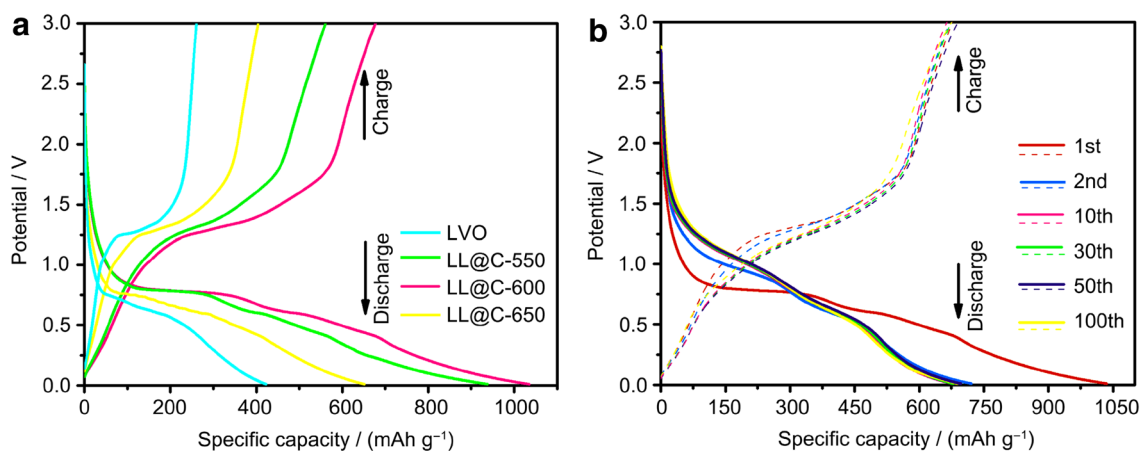
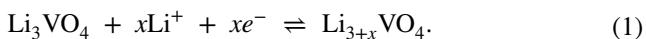


Fig. 5 **a** Initial charge–discharge curves of LVO, LL@C-550, LL@C-600 and LL@C-650 electrodes; **b** Galvanostatic charge–discharge voltage profiles of the LL@C-600 electrode for different cycles at a current density of 0.1 A g^{-1}

(Fig. 6). The positions of redox peaks of both samples are, however, slightly different. For Li_3VO_4 without a conductive layer, two obvious reduction peaks lie in the voltage of 0.496 and 0.805 V in the second cathodic scan, which are mainly related to the lithiation process (Eq. 1) [33, 34].



By contrast, for the sample with a conductive layer, both reduction peaks were shifted to 0.518 and 0.821 V, respectively. The higher lithiation voltage of LL@C-600 compared to that of LVO indicates a lower barrier potential, as concluded elsewhere [19, 28, 34]. For the anodic segment, the anodic peak of LVO at 1.386 V is attributed to the delithiation process of Eq. 1. Correspondingly, the oxidation peak of LL@C-600 is centered at 1.364 V. The voltage changes

between anodic and reduction peaks after the first cycles are provided in Table 1. The voltage changes of LL@C-600 displayed are obviously smaller than those of LVO, especially as the cycle progresses. This observation suggests that the sample with a conductive layer has lower polarization and faster Li^+ diffusion than that without a conductive layer. Similar cases were found elsewhere [26, 33, 34].

The cycling properties of all samples were assessed at a current density of 100 mA g^{-1} over the voltage window from 0.01 to 3 V, as shown in Fig. 7a. The comparison of the cycle property among LVO, LL@C-550, LL@C-600 and LL@C-650 electrodes indicates that LiVO_2 and carbon play an important role in improving the electrochemical performance. Compared to the sample without a surface conductive layer (LVO), LL@C-550, LL@C-600 and LL@C-650 showed an obvious increase in the specific capacity, among

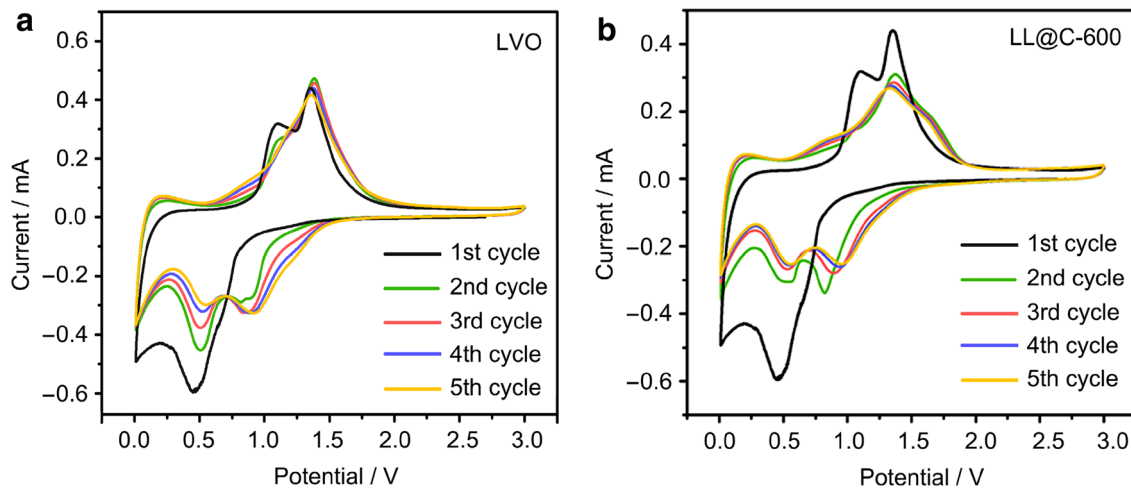


Fig. 6 Cycle voltammograms at a scan rate of 0.2 mV s^{-1} for the samples **a** LVO and **b** LL@C-600 in initial five cycles

Table 1 Voltage differences between anodic peaks and reduction peaks for samples LVO and LL@C-600 after the 1st cycle

Sample	Cycle	φ_0/V	φ_{r1}/V	φ_{r2}/V	$\Delta\varphi_{r1}/V$	$\Delta\varphi_{r2}/V$
LVO	2nd	1.386	0.496	0.805	0.890	0.581
	3rd	1.387	0.492	0.826	0.895	0.561
	4th	1.383	0.510	0.855	0.873	0.528
	5th	1.375	0.523	0.883	0.852	0.492
LL@C-600	2nd	1.364	0.518	0.821	0.846	0.543
	3rd	1.357	0.528	0.898	0.829	0.459
	4th	1.339	0.543	0.936	0.796	0.403
	5th	1.331	0.552	0.951	0.779	0.380

φ_0 oxidation peak, φ_{r1} the first reduction peak, φ_{r2} the second reduction peak, $\Delta\varphi_{r1} = \varphi_0 - \varphi_{r1}$; $\Delta\varphi_{r2} = \varphi_0 - \varphi_{r2}$

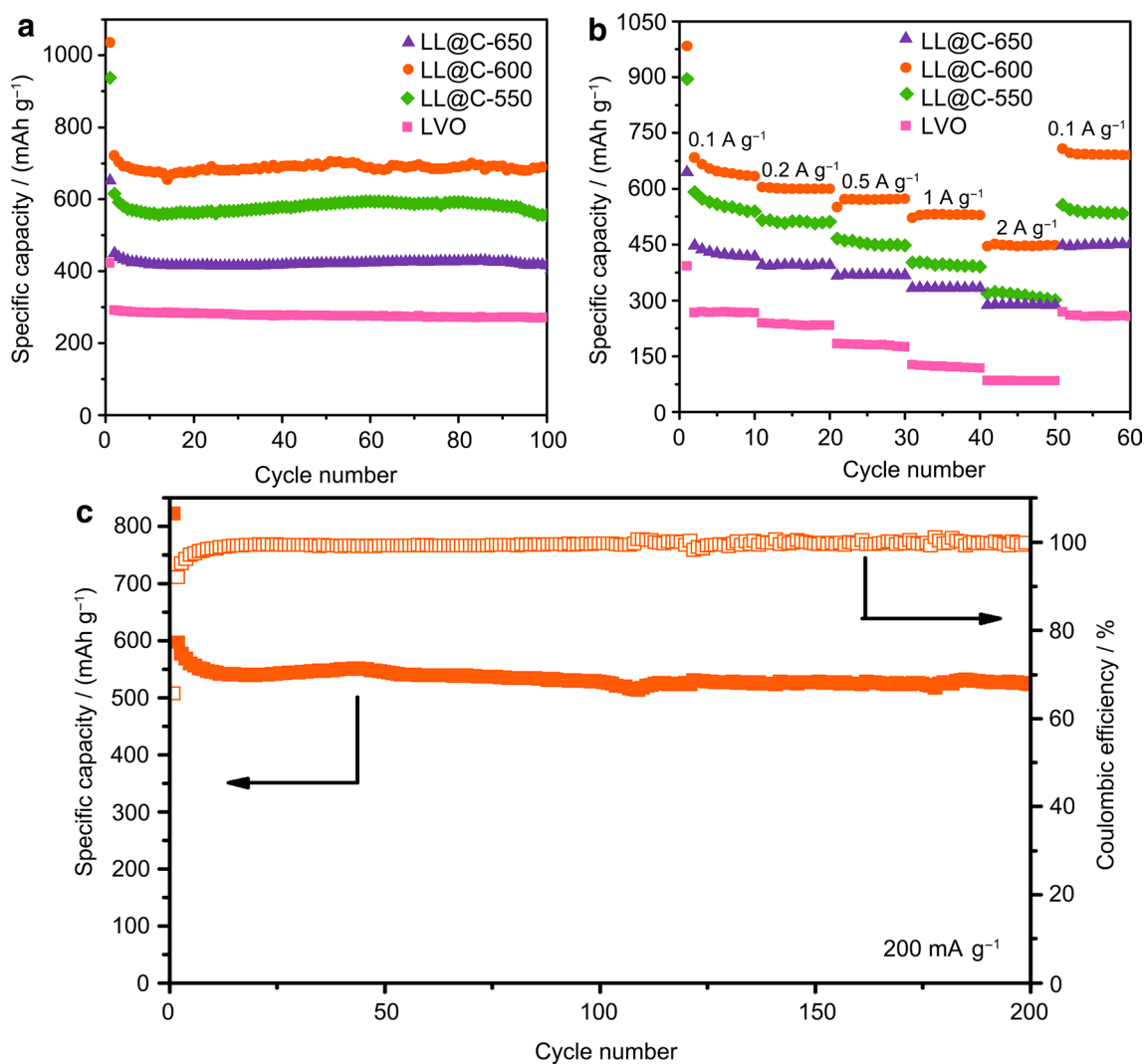


Fig. 7 Electrochemical properties of LVO, LL@C-550, LL@C-600, and LL@C-650 electrodes: **a** cycling performance at a current density of 100 mA g⁻¹; **b** rate capability at varied current densities; **c**

cycling ability, Coulombic efficiency of LL@C-600 at a current density of 200 mA g⁻¹

which LL@C-600 presents the optimum specific capacity. Besides, the initial Coulombic efficiency (CE) of LL@C-600 is 66%, which is higher than 62.2% for LVO, 60.7% for LL@C-550, and 62.8% for LL@C-650. The irreversible capacity fading in the 1st cycle of the LL@C-600 electrode is mainly due to the formation of the irreversible solid electrolyte interface (SEI) film and side reactions related to electrolyte [19, 33]. Notably, after the 100th cycle, the LL@C-600 electrode still showed a high discharge capacity of 689 mAh g^{-1} that reached 96% of the discharge capacity of the second cycles. The CE retained an average value of 97% among subsequent cycles, manifesting an outstanding reversibility of Li^+ in LL@C-600 electrode.

In sharp contrast, LVO demonstrates a specific capacity of only 273 mAh g^{-1} after 100 loops. Such an outstanding cycling ability for LL@C-600 is probably attributed to the synergistic effect of LiVO_2 and carbon. LiVO_2 is an excellent electronic and ionic conductor, which can significantly elevate the electronic conductivity and Li^+ ion diffusion coefficient of Li_3VO_4 . In the meantime, the introduction of carbonaceous matrix can not only improve the electronic conductivity and prevent the agglomeration of LVO particles, but also alleviate the volume change. As for LL@C-550 and LL@C-650, the initial discharge/charge capacity were 651 and 395 mAh g^{-1} , 938 and 589 mAh g^{-1} , respectively, which are far larger than those of the LVO anode. This observation also demonstrates that the existence of LiVO_2 and carbon matrix would obviously enhance the specific capacity. After 100 loops, the capacity retention for LL@C-550 and LL@C-650 is 105% and 94%, respectively, revealing an excellent cycling stability also.

To satisfy the rising demand of high-power devices, the superior rate capability of batteries is strongly aspired. Rate capability of LVO-based electrodes is displayed in Fig. 7b. The LL@C-600 electrode expresses a more superior rate capability compared with other electrodes. When the current densities are set at current densities of 0.1, 0.2, 0.5, 1

and 2 A g^{-1} , the capacities of the LL@C-600 anode are 634, 600, 573, 529 and 448 mAh g^{-1} , respectively, which are greater than those of other LVO anodes (267, 233, 175, 118, 84 mAh g^{-1} at rates of 0.1, 0.2, 0.5, 1 and 2 A g^{-1} , respectively). When the current density recovers to 0.1 A g^{-1} , a specific capacity of 690 mAh g^{-1} is observed, implying a superior reversibility. Besides these advantages, LL@C-650 sample presents a rate performance better than the pristine one, but does not appear as much improvement as the LL@C-550 electrode. The significantly improved rate capability could be the dual consequences of (i) rapid lithium-ion diffusion because of the good ionic conductivity of the conductive layer LiVO_2 and (ii) fast electron transfer due to the good electronic conductivity of the carbon matrix.

Figure 7c displays the cycling properties of all samples over a voltage window of 0.01–3 V vs. Li/Li^+ at a current density of 200 mA g^{-1} . When at a higher current density, the LL@C-600 sample still shows a high discharge capacity of 522 mAh g^{-1} with a retention rate of 92% after 200 cycles, and a stable CE of $98 \pm 2\%$ after the first three loops. Table 2 compares the electrochemical properties of the LL@C-600 anode with those previously reported for $\text{Li}_3\text{VO}_4/\text{C}$ based anodes. It appears that LL@C-600, when acts as an anode material for LIBs, exhibits the lithium storage performance superior to those ever reported in literature for LVO-related materials like LVO/C/rGO [11], LVO/C hollow spheres [16], mesoporous $\text{Li}_3\text{VO}_4/\text{C}$ supported on rGO [39], $\text{Li}_3\text{VO}_4\text{-BMC}$ [35] and LVO-m/c [29]. The excellent discharge capacity, longtime cycle stability and outstanding rate capability displayed by the LL@C-600 electrode could be attributed to the reasons below: (i) the conductive LiVO_2 layer is an ionic conductor that could dramatically improve Li^+ ion diffusion during cycling; (ii) Carbon is in situ formed during the calcination process that could be beneficial for fast electron transfer and inhibiting particle aggregation.

To figure out the possible factors responsible for the excellent rate capability, EIS was conducted to explore the

Table 2 Comparison of electrochemical performance of LL@C-600 and other LVO@C electrodes

Material	Initial discharge–charge capacity/(mAh g^{-1})	Capacity retention	Rate performance	Potential window/V	Reference
LVO/C/rGO	400/at 0.1 A g^{-1}	378 (100 cycles)	313 mAh g^{-1} at 2 A g^{-1}	0.2–3	[11]
LVO/C hollow spheres	660/430 at 0.1 A g^{-1}	400 (after 100 cycles at 0.08 A g^{-1})	350 mAh g^{-1} at 2 A g^{-1}	0.02–3	[16]
LVO	422/323 at 0.39 A g^{-1}	376 (after 75 cycles)	107 mAh g^{-1} at 1.9 A g^{-1}	0.01–3	[25]
Ca-doped Li_3VO_4	701/526 at 0.39 A g^{-1}	428 (180 cycles)	372 mAh g^{-1} at 1.5 A g^{-1}	0.01–3	[28]
Nb-doped Li_3VO_4	719/549 at 0.03 A g^{-1}	410 (100 cycles at 0.2 A g^{-1})	230 mAh g^{-1} at 1.5 A g^{-1}	0.01–3	[33]
$\text{Li}_3\text{VO}_4\text{-BMC}$	225/315 at 0.02 A g^{-1}	245 (after 50 cycles)	147 mAh g^{-1} at 0.3 A g^{-1}	0.05–3	[35]
$\text{Li}_3\text{VO}_4/\text{C}$	760/562 at 0.08 A g^{-1}	398 (after 80 cycles at 0.4 A g^{-1})	370 mAh g^{-1} at 3 A g^{-1}	0.01–3	[36]
HP- $\text{Li}_3\text{VO}_4/\text{C}$	450/390 at 0.2 A g^{-1}	370 (after 200 cycles at 0.2 A g^{-1})	300 mAh g^{-1} at 2 A g^{-1}	0.01–3	[37]
$\text{Li}_3\text{VO}_4/\text{C}$ nanofibers	548/451 at 0.04 A g^{-1}	394 (after 100 cycles)	141 mAh g^{-1} at 2 A g^{-1}	0.01–3	[38]
LL@C-600	1036/684 at 0.1 A g^{-1}	522 (after 200 cycles at 0.2 A g^{-1})	448 mAh g^{-1} at 2 A g^{-1}	0.01–3	This work

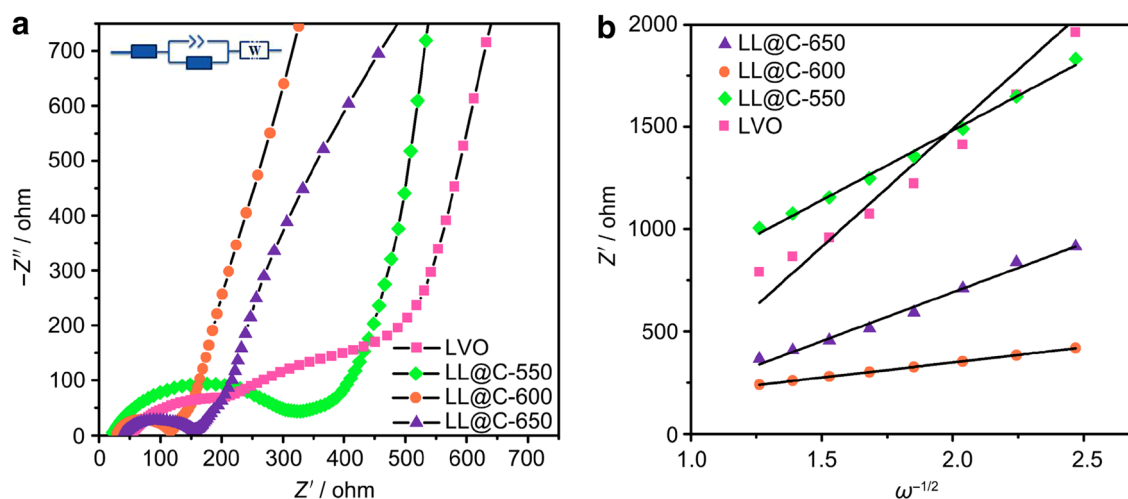


Fig. 8 **a** EIS plots and **b** Z' vs. $\omega^{-1/2}$ for samples LVO, LL@C-550, LL@C-600 and LL@C-650. Inset of **a** shows the corresponding equivalent circuit model

Table 3 Comparisons of impedance parameters for samples LVO, LL@C-550, LL@C-600, and LL@C-650

Sample	R_{ct}/Ω	Liner relation of Z' and $\omega^{-1/2}$ ($x: \omega^{-1/2}$; $y: Z'$)	$D_{Li}^+/(cm^2 s^{-1})$
LVO	350	$y = 1152x - 814$	7.32×10^{-18}
LL@C-550	275	$y = 680x + 121$	2.10×10^{-17}
LL@C-600	67	$y = 147x + 54$	4.50×10^{-16}
LL@C-650	88	$y = 476x + 262$	4.29×10^{-17}

electrochemical reaction kinetics. As shown in Fig. 8a, EIS plots of all electrodes consist of depressed semicircles and inclined lines. The impedance data were fit to a corresponding circuit, and the corresponding parameters are listed in Table 3. Apparently, the charge-transfer resistance (R_{ct}) value of LL@C-600 is 67 Ω , which is smaller than 88 Ω for LL@C-650, 275 Ω for LL@C-550, and 350 Ω for LVO. Much smaller R_{ct} value for LL@C-600 is exactly beneficial to the electron transfer and Li^+ diffusion during electrochemical processes. Li^+ diffusion during cycling was significantly improved by introduction of the conductive layer $LiVO_2$. Lithium diffusion coefficient (D_{Li}^+) could be evaluated according to the following Eq. 2:

$$D = R^2 T^2 / 2A^2 n^4 F^4 C^2 \sigma^2 \quad (2)$$

where R , A , T , n , C and F in the equation above represent the gas constant ($R = 8.314 \text{ J mol}^{-1} \text{ K}^{-1}$), electrochemical active surface area, absolute temperature ($T = 298 \text{ K}$), the number of electrons transferred during electrochemical processes, Faraday constant ($F = 96500 \text{ C mol}^{-1}$), molar

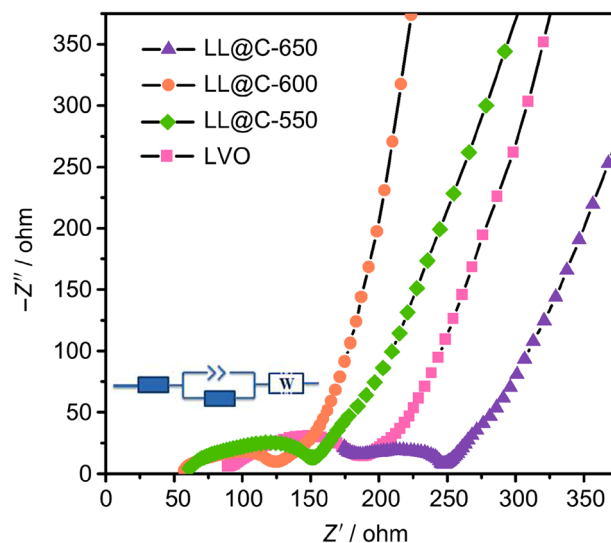


Fig. 9 EIS spectra of electrodes LVO, LL@C-550, LL@C-600, and LL@C-650 after 100 cycles, and the corresponding equivalent circuit model is inserted

Table 4 The impedance fitting parameters for samples LVO, LL@C-550, LL@C-600, and LL@C-650 after 100 cycles at 100 mA g^{-1} (Ω)

LVO	LL@C-550	LL@C-600	LL@C-650
110	97	85	100

concentration of Li^+ ions ($C = 9.8 \times 10^{-3} \text{ mol cm}^{-3}$), respectively, and the Warburg factor (σ) are able to be obtained from Eq. 3,

$$Z_{\text{re}} = R_{\text{ct}} + R_{\text{s}} + \sigma\omega^{-1/2} \quad (3)$$

The linear fitting plots of Z_{re} vs. $\omega^{-1/2}$ are displayed in Fig. 8b. The obtained Li^+ diffusion coefficient of LL@C-600 is 4.50×10^{-16} , which is around two orders of magnitude higher than that of 7.32×10^{-18} for LVO.

The apparently reduced R_{ct} and enhanced D_{Li}^+ for LL@C-600 manifest an optimum rate performance relative to other samples, consistent with our electrochemical performance results. Furthermore, from the comparison of Nyquist plots of LVO, LL@C-550, LL@C-600 and LL@C-650 after 100 loops at a current density of 100 mA g^{-1} in Fig. 9, it is concluded that LL@C-600 has a superior charge-transfer ability during cycles, since after the 100th cycle, R_{ct} of LL@C-600 is 85Ω , which is smaller than 97Ω for LL@C-550, 100Ω for LL@C-650, and 110Ω for LVO (Table 4).

4 Conclusion

This work reports on the synthesis of Li_3VO_4 with a conductive layer LiVO_2 and carbon matrix via one-step freeze-drying followed by a treatment at high temperatures in the inert atmosphere. The primary results could be summarized as follows: (i) The presence of the conductive layer on Li_3VO_4 boosted Li^+ diffusion during the electrochemical process; (ii) In situ formation of carbon during treatment in the inert atmosphere elevated the electronic conductivity, and inhibited the particle agglomeration; (iii) After treatment at $600 \text{ }^\circ\text{C}$, Li_3VO_4 with a conductive layer LiVO_2 showed an optimum lithium storage capability, including the excellent discharge capacity, longtime cycle stability and outstanding rate capability when compared to that without a conductive layer; (iv) Through systematic sample characterizations, the excellent electrochemical performance at the presence of the conductive layer was demonstrated to be the consequence of fast electron transfer and rapid Li^+ ion diffusion. The findings reported here may have a broad impact on exploring Li_3VO_4 and relevant vanadate materials for applications in next-generation lithium-ion batteries.

Acknowledgements This work was financially supported by the National Natural Science Foundation of China (Grant Nos. 21571176, 21671077, 21771075 and 21871106).

References

- Kong H, Wu Y, Hong W, Yan C, Zhao Y, Chen G. Structure-designed synthesis of Cu-doped Co_3O_4 @N-doped carbon with interior void space for optimizing alkali-ion storage. *Energy Storage Mater.* 2019. <https://doi.org/10.1016/j.ensm.2019.06.015>.
- Zhang D, Xi S, Li G, Li B, Fan J, Liu X, Chen D, Li L. Facile synthesis of $\text{Mn}_{2.1}\text{V}_{0.9}\text{O}_4/\text{rGO}$: A novel high-rate anode material for lithium-ion batteries. *J Power Sources.* 2019;426:197.
- Liu Y, Chen Z, Jia H, Xu H, Liu M, Wu R. Iron-doping-induced phase transformation in dual-carbon-confined cobalt diselenide enabling superior lithium storage. *ACS Nano.* 2019;13(5):6113.
- Zhu Z, Tang Y, Leow W, Xia H, Lv Z, Wei J, Ge X, Cao S, Zhang Y, Zhang W, Zhang H, Xi S, Du Y, Chen X. Approaching the lithiation limit of MoS_2 while maintaining its layered crystalline structure to improve lithium storage. *Angew Chem Int Ed.* 2019;58(11):3521.
- Li X, Li K, Zhu SC, Fan K, Lyu L, Yao H, Li Y, Hu J, Huang H, Mai YW, Goodenough JB. Fiber-in-tube design of Co_9S_8 -carbon/ Co_9S_8 : enabling efficient sodium storage. *Angew Chem Int Ed.* 2019;58(19):1.
- Hwang S, Yao Z, Zhang L, Fu M, He K, Mai L, Chris W, Su D. Multistep lithiation of tin sulfide: an investigation using in situ electron microscopy. *ACS Nano.* 2018;12(4):3638.
- Wei X, Wang X, Tan X, An Q, Mai L. Nanostructured conversion-type negative electrode materials for low-cost and high-performance sodium-ion batteries. *Adv Funct Mater.* 2018;28(46):1804458.
- Yan Z, Guo J. High-performance silicon-carbon anode material via aerosol spray drying and magnesiothermic reduction. *Nano Energy.* 2019;63:103845.
- Zhang D, Li G, Yu M, Fan J, Li B, Li L. Facile synthesis of $\text{Fe}_4\text{N}/\text{Fe}_2\text{O}_3/\text{Fe}$ /porous N-doped carbon nanosheet as high-performance anode for lithium-ion batteries. *J Power Sources.* 2018;384:34.
- Deng J, Yu X, Qin X, Zhou D, Zhang L, Duan H, Kang F, Li B, Wang G. Co-B nanoflakes as multifunctional bridges in ZnCo_2O_4 micro-/nanospheres for superior lithium storage with boosted kinetics and stability. *Adv Energy Mater.* 2019;9(14):1803612.
- Liu H, Hu P, Yu Q, Liu Z, Zhu T, Luo W, Zhou L, Mai L. Boosting the deep discharging/charging lithium storage performances of Li_3VO_4 through double-carbon decoration. *ACS Appl Mater Interfaces.* 2018;10(28):23938.
- Huang Y, Yang H, Zhang Y, Zhang Y, Wu Y, Tian M, Chen P, Trout R, Ma Y, Wu TH, Wu Y, Liu N. A safe and fast-charging lithium-ion battery anode using MXene supported Li_3VO_4 . *J. Mater. Chem. A.* 2019;7:11250.
- Dompablo MEA, Tartaj P, Amarilla JM, Amador U. Computational investigation of Li insertion in Li_3VO_4 . *Chem Mater.* 2016;28(16):5643.
- Zeng J, Yang Y, Li C, Li J, Huang J, Wang J, Zhao J. Li_3VO_4 : an insertion anode material for magnesium ion batteries with high specific capacity. *Electrochim Acta.* 2017;247:265.
- Liang Z, Zhao Y, Ouyang L, Dong Y, Kuang Q, Lin X, Liu X, Yan D. Synthesis of carbon-coated Li_3VO_4 and its high electrochemical performance as anode material for lithium-ion batteries. *J Power Sources.* 2014;252:244.
- Yang Y, Li J, He X, Wang J, Sun D, Zhao J. A facile spray drying route for mesoporous $\text{Li}_3\text{VO}_4/\text{C}$ hollow spheres as an anode for long life lithium ion batteries. *J. Mater. Chem. A.* 2016;4:7165.
- Liao C, Wen Y, Shan B, Zhai T, Li H. Probing the capacity loss of Li_3VO_4 anode upon Li insertion and extraction. *J Power Sources.* 2017;348:48.
- Ni S, Zhang J, Ma J, Yang X, Zhang L. Superior electrochemical performance of $\text{Li}_3\text{VO}_4/\text{N}$ -doped C as an anode for Li-ion batteries. *J. Mater. Chem. A.* 2015;3(35):17951.
- Liu X, Li G, Zhang D, Chen D, Wang X, Li B, Li L. Fe-doped Li_3VO_4 as an excellent anode material for lithium ion batteries: optimizing rate capability and cycling stability. *Electrochim Acta.* 2019;308:185.

20. Shen L, Chen S, Maier J, Yu Y. Carbon-coated Li_3VO_4 spheres as constituents of an advanced anode material for high-rate long-life lithium-ion batteries. *Adv Mater.* 2017;29(33):1701571.
21. Kang T, Shen D, Ni S, Chen Q, Li T, Yang X, Zhao J. Pseudocapacitive charge storage induced by self-enhanced electrical conductivity and Li-ion diffusion in high performance Li_3VO_4 @ LiVO_2 anode for Li-ion batteries. *J Alloy Compd.* 2018;741:442.
22. Li X, Su Z, Tian H, Zhang Y. Rhombohedral-structured LiVO_2 prepared by a novel two step method and its electrochemical properties. *Int J Electrochem Sci.* 2017;12:693.
23. Armstrong AR, Lyness C, Panchmatia PM, Islam MS, Bruce PG. The lithium intercalation process in the low-voltage lithium battery anode $\text{Li}_{1-x}\text{V}_{1-x}\text{O}_2$. *Nature Mater.* 2011;10:223.
24. Liu X, Zhang D, Li G, Xue C, Ding J, Li B, Chen D, Li L. In situ synthesis of V_2O_3 nanorods anchored on reduced graphene oxide as high-performance lithium ion battery anode. *ChemistrySelect.* 2018;3(43):12108.
25. Zhou LL, Shen SY, Peng XX, Wu LN, Wang Q, Shen CH, Tu TT, Huang L, Li JT, Sun SG. New insights into the structure changes and interface properties of Li_3VO_4 anode for lithium-ion batteries during the initial cycle by in-situ techniques. *ACS Appl Mater Interfaces.* 2016;8:23739.
26. Zhang CK, Liu CF, Nan XH, Song HQ, Liu YG, Zhang CP, Cao GZ. Hollow-cuboid $\text{Li}_3\text{VO}_4/\text{C}$ as high-performance anodes for lithium-ion batteries. *ACS Appl Mater Interfaces.* 2016;8(36):680.
27. Zhang C, Wang K, Liu C, Nan X, Fu H, Ma W, Li Z, Cao G. Effects of high surface energy on lithium-ion intercalation properties of Ni-doped Li_3VO_4 . *NPG Asia Mater.* 2016;8:e287.
28. Zhou J, Zhao B, Song J, Chen B, Ma X, Dai J, Zhu X, Sun Y. Optimization of rate capability and cyclability performance in Li_3VO_4 anode material through Ca doping. *Chem Eur J.* 2017;23(64):16338.
29. Xu X, Niu F, Wang C, Li Y, Zhao C, Yang J, Qian Y. Li_3VO_4 nanoparticles in N-doped carbon with porous structure as an advanced anode material for lithium-ion batteries. *Chem Eng J.* 2019;370:606.
30. Yang Y, Li J, Huang J, Huang J, Zeng J, Zhao J. Polystyrene-template-assisted synthesis of $\text{Li}_3\text{VO}_4/\text{C}/\text{rGO}$ ternary composite with honeycomb-like structure for durable high-rate lithium ion battery anode materials. *Electrochim Acta.* 2017;247:771.
31. Zhang D, Li G, Li B, Fan J, Chen D, Liu X, Li L. Fast synthesis of $\text{Co}_{1.8}\text{V}_{1.2}\text{O}_4/\text{rGO}$ as a high-rate anode material for lithium-ion batteries. *Chem. Commun.* 2018;54:7689.
32. Zhang D, Li G, Fan J, Li B, Li L. Tuning shell thickness of MnO/C core-shell nanowires for optimum performance of lithium-ion batteries. *Chem Res Chin Univ.* 2017;33(6):924.
33. Zhao L, Duan H, Zhao Y, Kuang Q, Fan Q, Chen L, Dong Y. High capacity and stability of Nb-doped Li_3VO_4 as an anode material for lithium ion batteries. *J Power Sources.* 2018;378:618.
34. Wang K, Fu H, Li Z, Xia M, Liang X, Qi R, Cao G, Lu X. Enhancing the rate performance of a Li_3VO_4 anode through Cu doping. *ChemElectroChem.* 2018;5(3):478.
35. Li Q, Wei Q, Sheng J, Yan M, Zhou L, Wen L, Sun R, Mai L. Mesoporous $\text{Li}_3\text{VO}_4/\text{C}$ submicron-ellipsoids supported on reduced graphene oxide as practical anode for high-power lithium-ion batteries. *Adv. Sci.* 2015;2(12):1500284.
36. Shao G, Gan L, Ma Y, Li H, Zhai T. Enhancing the performance of Li_3VO_4 by combining nanotechnology and surface carbon coating for lithium ion batteries. *J. Mater. Chem. A.* 2015;3:11253.
37. Liang ZY, Zhao YM, Dong YZ, Kuang Q, Lin XH, Liu XD, Yan DL. The low and high temperature electrochemical performance of $\text{Li}_3\text{VO}_4/\text{C}$ anode material for Li-ion batteries. *J Electroanal Chem.* 2015;745:1.
38. Zhao D, Cao MH. Constructing highly graphitized carbon-wrapped Li_3VO_4 nanoparticles with hierarchically porous structure as a long life and high capacity anode for lithium-ion batteries. *ACS Appl Mater Interfaces.* 2015;7:25084.
39. Qin RH, Shao GQ, Hou JX, Zheng Z, Zhai TY, Li HQ. One-pot synthesis of $\text{Li}_3\text{VO}_4/\text{C}$ nanofibers by electrospinning with enhanced electrochemical performance for lithium-ion batteries. *Sci Bull.* 2017;62:1081.

Publisher's Note Springer Nature remains neutral with regard to jurisdictional claims in published maps and institutional affiliations.



Prof. Guangshe Li is the director of State Key Lab of Inorganic Synthesis and Preparative Chemistry, Jilin University. Dr. Li obtained his Ph.D. degree from Jilin University in 1997. Then, he had worked as a postdoc in Xi'an Jiaotong University for 2 years. After that, he moved to Tohoku University, Japan and Brigham Young University, USA to continue his postdoc research. At the beginning of 2004, he returned to China, elected as "Hundreds of Talent Program" of Chinese Academy of Science

(CAS), and worked as a full professor in Fujian Institute of Research on the Structure of Matter (FJIRSM). In 2015, he moved to Jilin University as a professor. He was supported by "National outstanding Youth Program" of National Natural Science Foundation of China (NSFC). Till now, he published over 260 papers with a H index of 51.